Quenching a swarm: Effect of light exposure on suppression of collective motility in swarming *Serratia marcescens*

Alison E. Patteson[1,‡], Paulo E. Arratia[2] and Arvind Gopinath[3,‡]
[1]*Department of Physics, Syracuse University, Syracuse, NY.*
[2]*Department of Mechanical Engineering & Applied Mechanics, University of Pennsylvania, Philadelphia, PA 19104.*
[3]*Department of Bioengineering, University of California Merced, CA 95340.*
[‡]*aepattes@syr.edu, agopinath@ucmerced.edu*

Swarming colonies of the light sensitive bacteria *Serratia marcescens* grown on agar exhibit robust, fluctuating, collective flows that include vortices, jets and sinuous streamers spanning multiple bacterial lengths. Here, we study the effects of light with a substantial ultra-violet component on these collective flows. We explore two features of the response to high intensity light: (i) the reversible versus irreversible nature of the bacterial response and (ii) the effects of exposure time and light intensities on the growth rate of the paralyzed region during exposure and its dissolution rate post-exposure. For small exposure times and low intensities, we find collective mobility to be negligibly affected. Increasing exposure times and/or intensity to higher values temporarily suppresses collective mobility. However, when exposure is stopped, bacteria regain motility at the single cell level and eventually reestablish large scale flows. For long exposure times or high intensities, exposed bacteria become paralyzed and in the process form jammed, highly aligned domains. Post exposure, unexposed bacteria dislodge exposed bacteria from these caged configurations; consequently, the dissolution rate upon cessation of exposure depends on duration of exposure. Our results complement previous studies on the effects of light on planktonic bacteria and inform models of light-driven patterning in clusters of deactivating bacteria.

I. INTRODUCTION

Swarming motility is a flagella driven form of bacterial surface migration that allows for rapid colonization of environments [1–8]. Widespread in both Gram-positive and Gram-negative bacteria [3, 8], swarming is usually observed when free-swimming (planktonic) bacteria grown in fluids are subsequently transferred to soft wet agar gels [5]. The transfer triggers a change in phenotype; individual cells become significantly elongated and the number of flagella increases to 10–100 [1, 7]. At high densities, the colony develops complex, long-range intermittent collective flow features that involving multiple bacteria traveling in rafts or flock-like clusters. The velocity fields are most prominent and intense near the edge of the expanding colony with intensity decreasing far from the propagating edge [2, 4, 5, 9]. Recent studies [10–12] demonstrate that swarming confers multiple benefits including enhanced colonization rates and elevated resistance to antibiotics when compared to other forms of bacterial motility. Swarming is also found to be co-regulated with virulence, and implicated in infectiousness and fitness of pathogenic bacterial species [3, 7].

Healthy bacterial cells sense spatiotemporally distributed cues, continuously process these inputs and transduce them to variations in motility and other responses [1, 4, 9, 13]. The effects of external stimuli including light have been studied in free-swimming (planktonic) bacteria; for instance, free-swimming bacteria are observed to respond to external stimuli by modulating and controlling the molecular motors underlying flagellar motion [14–18]. Intense light with wavelengths in the range 290-530 nm encompassing the ultraviolet (UV) range is known to trigger changes in the motility of planktonic chemotactic bacteria [19–21]. Prolonged exposure to high-intensity light results in progressively slow swimming with paralysis occurring eventually [19, 20] due to irreversible motor damage. Changes in motility of *Escherichia coli* and *Streptococcus* are hypothesized to arise from controlled variations in the tumble frequency, a behavior that requires requires the chemotaxis signal protein CheY [20, 22].

From a medical perspective, light treatments employing UV-A, UV-B and UV-C radiation are emerging as attractive alternatives to antibiotic treatment of pathogenic bacteria. Light exposure is known to inhibit cell growth and induce gene damage [23] in marine organisms (alphaprotobacteria and bacterioplankton, [24]), airborne bacteria [25], as well in bacterial biofilms [26, 27]. Irradiation of surfaces using blue light and phototherapy that activates endogenous or exogenous photosensitizers [13, 28, 29] has been shown to sterilize and disinfect bacteria laden surfaces. Swarming bacteria are susceptible to light in the presence of photosensitizer [13, 30] which disrupts the swarm motility by releasing reactive oxygen species (similar to other photosensitizing dyes). The effect of light on *Bacillus subtilis* [30] in the presence of photosensitizer reveals that as the bacterial cells become sluggish, the tendency to form flocks and large packs reduces and instead smaller clusters are observed. The overall reduction in cluster size and a less ordered motion within individual clusters gives rise to decreased correlation lengths with swarming eventually reverting to random motion in the presence of photodynamic effects.

During exposure, the collective swarm velocity decays, a feature that can be recovered after exposure. Intense light is also known to promote wound healing [29, 31] with visible light recently approved to treat bacterial infections such as acne [32].

Given these promising studies and the timeliness of light treatments, understanding the connection between motility, infectiousness and light exposure is particularly important. However, significant challenges remains in uncovering the role of external stimuli such as light in modulating relationships between the onset of collective motion and motility at the single cell level. Similar questions arise in studies on chemotactic bacteria where modulation in the functioning of the MotA - MotB pair and FliG comprising the rotary motor complex in bacterial flagella is observed during chemotaxis. At the organismal scale, the net result is change in the trajectory - specifically, tumble length and turning frequency - that directs them towards nutrients and away from toxins [15, 17]. These changes may then be transduced into changes at the collective level by accompanying changes in cell-cell interactions.

In this article, we report on the effects of wide-spectrum light with a significant UV component on the swarming dynamics of *Serratia marcesens*. In collectively-moving swarms, individual self-propelling cells are influenced by steric and hydrodynamic interactions with their neighbors [4–6, 33, 34]. These interactions result in collective (macroscopic) speeds being different from the self-propulsion speed i.e., the speed of an isolated cell and result in complex features such as fluctuating regions of high vorticity. We first discuss statistics of unexposed bacterial swarms. Then we present results obtained by exposing localized regions of the swarm to wide-spectrum light and systematically identify exposure times and light intensities that paralyze the active swarm and render bacteria immotile. This *quenching* of activity may happen in either reversible or irreversible manner. In addition to the direct effects of light such as reduced speed, there are secondary effects, including the creation of dense strongly jammed domains of immobile cells as the results of sustained exposure. These dense immobile domains hinder the penetration of unexposed bacteria into the region, thereby reducing total damage to bacteria in the colony. Post-exposure, swarming cells penetrate into the previously passive domain slowly, dislodging and convecting immobile bacteria away. The rate at which the dissolution proceeds in its initial stages depends on the degree of jamming (caging) of the exposed region and therefore on the strength and duration of light exposure. We observe that bacteria exposed to sufficiently low light intensities recover their motility and erode the passive domain from within. Finally, using a simple agent based Brownian dynamics model of a slowly diffusing and deactivating cell, we show how changes in diffusivity and activity (self-propulsion speed) results in variations in bacterial spreading distances.

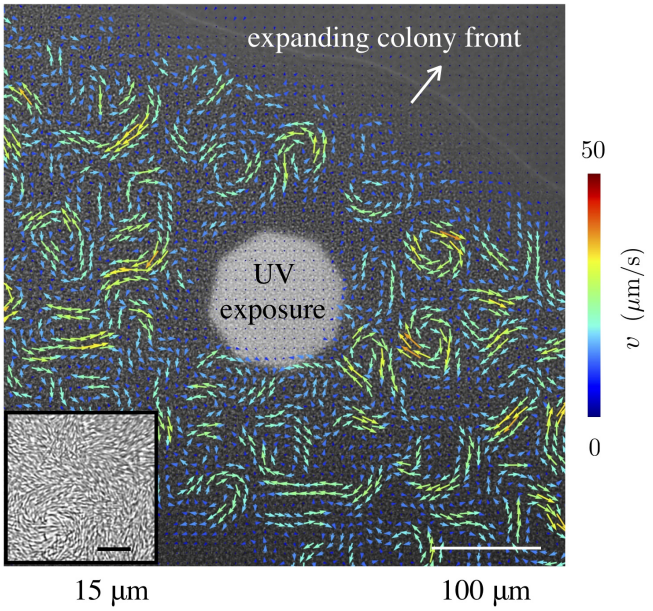

FIG. 1. **Characteristics of swarming and expanding colony:** Snapshot of a *Serratia marcescens* colony on an agar substrate, during exposure to high-intensity light from a mercury lamp source; PIV derived velocity fields are overlaid in color. Swarming motion is pronounced approximately 50 microns from the expanding colony front. The inset shows pre-exposure bacterial alignment and density 150 μm from the colony front.

II. EXPERIMENTAL METHODS

Swarms of *Serratia marcesens* (strain ATCC 274, Manassas, VA) were grown on agar substrates, prepared by dissolving 1 wt% Bacto Tryptone, 0.5 wt% yeast extract, 0.5 wt% NaCl , and 0.6 wt% Bacto Agar in deionized water. Melted agar was poured into petri dishes, adding 2 wt% of glucose solution (25 wt%). The bacteria were then inoculated on solidified agar plates and incubated at 34°C. Colonies formed at the inoculation sites and grew outward on the agar substrate from the inoculation site.

Swarms were studied and imaged 12-16 hours after inoculation. The bacteria were imaged with the free surface facing down with an inverted Nikon microscope Eclipse Ti-U using either a Nikon 10x (NA = 0.3) or 20x (NA = 0.45) objective. Images were gathered at either 30 frames per seconds with a Sony XCD-SX90 camera or at 60 frames per second with a Photron Fastcam SA1.1 camera. We used videos of the swarm and PIVLab software [35] to extract the velocity fields of the bacteria with particle image velocimetry (PIV) techniques. Particle image velocimetry determines velocity fields by calculating local spatial-correlations between successive images. Here, the images are of bacteria (either active or passive) such that PIV yields the bacterial velocity fields directly and not the velocity field of the ambient fluid. We sampled the velocity field at 3 μm spatial intervals of images; we checked the frame rate for accurate resolution.

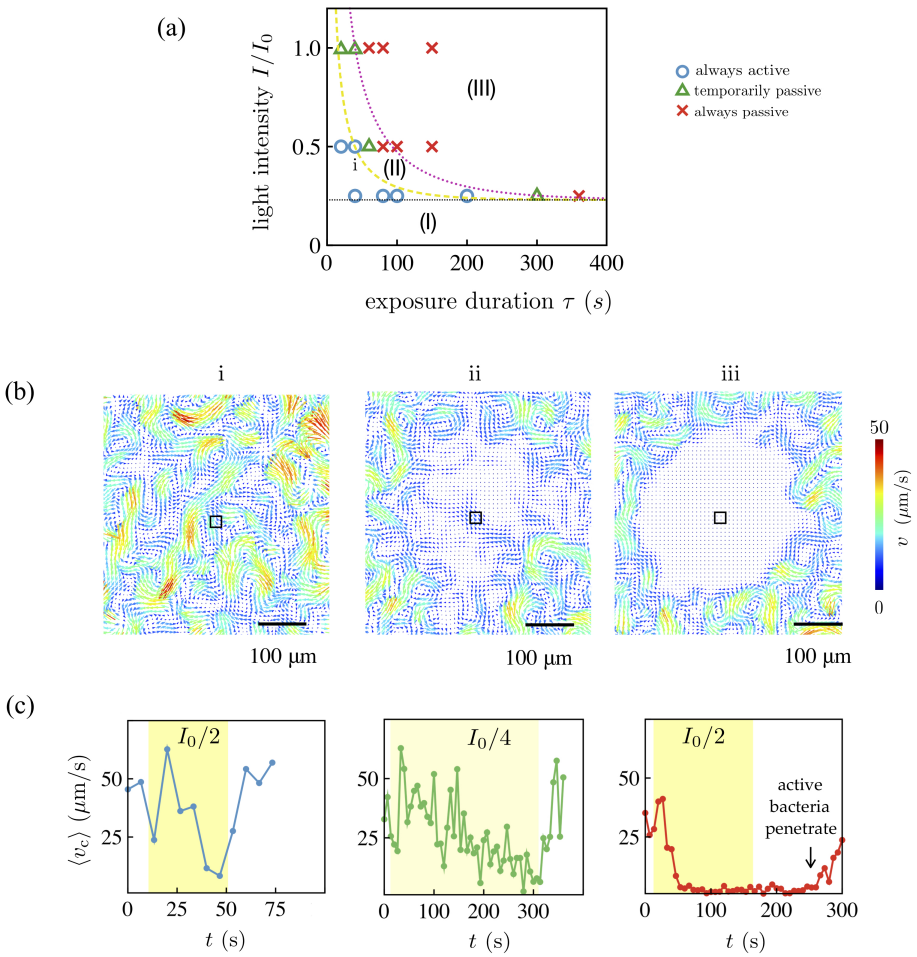

FIG. 2. **Phase space for collective motility after exposure:** (a) Changes in collective flows (relative to the unexposed state) in swarming *Serratia marcescens* depend strongly on intensity and duration of light exposure. We use a wide spectrum mercury lamp (bare intensity $I_0 = 980$ mW/cm^2 at 535 nm) with filters to selectively expose regions of the swarm to a filtered maximum intensity I. From subsequent PIV analysis of bacterial velocities, the response can be classified into one of three types - (I) always active, (II) temporarily passive, and (III) always passive. The yellow (dashed) and pink (dotted) curves are phase boundaries predicted by equation 1. (b) Velocity fields taken 10 s post exposure are shown for each phase. Colors reflect speed with the arrows denoting polar orientation. Collective motility of temporarily immobile bacteria is recovered in approximately 15 seconds past exposure. (c) We plot the average speed of the swarm in the central region, highlighted by the box in (b) for times encompassing pre-exposure, exposure (yellow band), and post-exposure. Pre-exposure, the average swarm speed fluctuates between 25 to 50 μm/s. For case (I), the bacteria briefly slow down during exposure, but recover in 6 s. In (II), the swarm speed approaches zero during exposure and recovers in 12s. In (III), the collective swarm speed drops to and remains zero.

To mimic the exposure of bacteria to naturally occurring high intensity light, a wide spectrum mercury vapor lamp[36] and standard microscope optics were used to focus the light on the swarm. The bare unfiltered maximum intensity (measured at 535 nm) of the lamp I_0 was reduced to lower, filtered (maximum) intensities I using neutral density filters. Both I_0 and I depend on the objective: using a spectrophotometer (Thorlabs, PM100D), we measured intensities $I_0 = 980$ mW/cm^2 (at 535 nm) for the 10x and $I_0 = 3100$ mW/cm^2 (at 535 nm) for the 20x objectives. Note that the actual intensity of light $I^*(\mathbf{r}, t)$ as measured in the swarm is spatiotemporally varying due to bacterial motion and also due to the associated point spread distribution as the light passes through the aperture.

III. RESULTS AND DISCUSSION

A. Collective motility - exposed and unexposed regions

Figure 1 shows the expanding edge of the colony, a region of which (white area, exposed using an octagonal aperture) is exposed to high-intensity light from a mercury vapor lamp [36]. The swarm is expanding from

left to right; the colony edge is indicated in white in the figure. Bacteria swim in a thin layer above the agar substrate (inset, Figure 1). The thickness of the swarm varies with distance from the leading edge: studies on *E. coli* [37] showed that cells form a monolayer over a significant region close to the leading edge, beyond this cells can form multi-layered regions. Overlaid on the image in Fig. 1 are bacterial velocity fields gathered from PIV; the image is taken after 80 seconds of exposure. Outside of the exposed region, the velocity field exhibits long-range collective flows. Unexposed bacteria move fastest approximately 100-400 μm from the colony edge (maximum speeds $\sim$80 μm/s, average speed $\sim$30 μm/s). In contrast, inside the exposed region, the bacterial motility is significantly impaired. This is evident in SI-Movie 1; as swarming bacteria are exposed to light, they slow down and are eventually trapped within the exposed region. This feature is reflected in the trajectories of the small tracer-like as they slow down and eventually stop moving when trapped amongst the passive bacteria. The interphase boundary between the unexposed (passive) domain and the unexposed (active) part of the swarm features strong vortices, jets, and streamers, extending up to just a few microns away from the exposed domain.

B. Phase-space for collective motility

The quenching (passivation) of collective mobility of the initially active bacteria is not immediate and can be reversible depending on the intensity of light. In the experiment corresponding to Fig. 1, the exposed bacteria remain passive even after the wide-spectrum mercury lamp is switched off. In the absence of the light, the passivated domain does not retain its shape or size; it is unstable and erodes as active swarming bacteria penetrate the passive domain and convect passive bacteria away. Based on these observations, we explore two features of the response to high intensity light: (i) the reversible versus irreversible nature of the bacterial response and (ii) the effects of exposure time and light intensities on the passive domain growth rate during exposure and dissolution rate post-exposure.

Figure 2 illustrates three different types of bacterial response to light for varying exposure times and intensities. We classify the response types based on the time-dependent velocity fields of the swarm: exposed cells either (i) retain mobility with negligible effects, (ii) transiently stop moving, or (iii) permanently stop moving. To quantify the response, the phase behavior was mapped onto a phase diagram with exposure time τ and light intensity I (varied from the bare value I_0 using neutral density filters) as variables. For sufficiently small exposure times ($\tau \sim 20-40$ s) and intensities ($I < 220$ mW, at 535 nm), exposed cells remain always active. Conversely, for large exposure times ($\tau > 60$ s) and sufficiently high intensities ($I > 220$mW, at 535 nm), the bacteria are permanently passive (over the duration of the experiment).

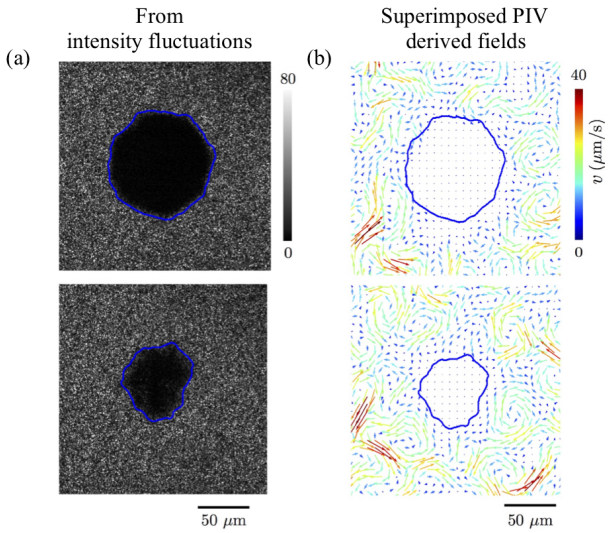

FIG. 3. **Thresholding using intensity fluctuation fields:** (a) We calculate an intensity fluctuation map $|I^*(\mathbf{r}, t+\Delta t) - I^*(\mathbf{r}, t)|$, with $\Delta t = 0.1$ seconds. Intensity fluctuations are low (black, third tile from left) in the regions where the swarm is not moving. The map when thresholded allows us to identify the boundary position (blue contours). The passive phase shrinks as time goes by as shown at $t = 1$ sec (top) and $t = 40$ sec (bottom) post-exposure (Exposure duration $\tau = 80$ sec, Intensity is 3 W/cm^2 measured at wavelength 535 nm). (b) PIV derived bacteria velocity fields confirm the boundary location obtained from the intensity fluctuation maps. A mathematically defined diffuse boundary may be obtained from phase field profiles [38] using order parameters [39]; here however, we use simple thresholding.

As seen in Fig. 2(a), between these two phases lies the temporarily passive, reversible case.

The differences between the three (collective) motility regimes are highlighted in Fig. 2(b) and (c); these show PIV-derived velocity fields taken 10 seconds past exposure (Fig 2b) and the average bacterial speed $\langle v_c \rangle$ - in the exposed region - over time (Fig 2c). Here, $\langle v_c \rangle$ is the average speed of the velocity fields in a 22×22 μm^2 area, located at the center of the exposed region. In case (i), exposed cells remain motile and continue to exhibit long-range collective motions; the speed decreases but does not fully reach zero during exposure. The speed recovers to pre-exposure levels approximately 5 seconds after exposure. In case (ii), bacteria stop moving during exposure, yet spontaneously start moving again $\sim$ 1-10 s after the light is switched off. The cell speed $\langle v_c \rangle$ takes longer to recovers to pre-exposure levels than case (i), and the recovery occurs heterogeneously with cells moving within the temporally-quiescent region (Fig. 2(b)-ii). This process superficially resembles the heterogeneous, disconnected melting of a large frozen domain. In case (iii), cells stop moving during exposure and do not regain their motility afterward for the whole duration of the experiment (20-300 s). Unlike case (ii), cells in the exposed region here do not spontaneously regain their motility

(Fig. 2(b)-iii). We find that, in this case, the passive domain evolves solely due to its interaction with the active swarm at its boundary. The active swarm convects passive bacteria away from the boundary and the passive phase is dismantled entirely; the speed $\langle v_c \rangle$ eventually increases (Fig. 2(c)-iii) as the swarm recaptures the quenched area. Similar responses have been observed earlier in studies on *E. coli* and *S. typhimurium* [19]. Specifically, prolonged exposure to unfiltered light in both bacterial species resulted in constant tumbling, then smooth swimming, and eventually paralysis. *S. typhimurium* was found to responds instantaneously to exposure with recovery of normal motility in 2 s or less upon cessation of exposure provided the duration of exposure was less than 5s. Similarly, *E. coli* recovered normal motility in 1 to 10 s after cessation of exposure. Sustained exposure that ultimately results in paralysis was however found to be irreversible (with no recovery of motility even after 15 minutes) for both species.

The regimes in the phase-plot Figure 2(a) can be rationalized by assuming the existence of a lower threshold for the intensity $I_{\rm min}$ below which bacteria are not affected. We note that the curves separating these regions of phase space do not correspond to a single or unique value of the light dosage (intensity multiplied by exposure time) or net power. The response to light involves changes to the motor complex and possibly involves a cascade of biochemical events. At the same time, while active swarming bacteria swim in and out of the exposed region close to the edge; in the interior of the exposed region they are caged in by their neighbors. To interpret Figure 2, we treat these independent motility affecting mechanisms in an approximate phenomenological way using a lumped time approximation. We invoke an intrinsic time scale τ_* that determines the internal organismal response to light (here quantified using the maximum of the filtered intensity) resulting in either temporary ($\tau_* = \tau_{\rm temp}$) or permanent ($\tau_* = \tau_{\rm perm}$) passivation. The curves that separate the different responses in Figure 2(a) may then be fit by

$$\frac{I(\tau)}{I_0} = A \exp(-\frac{\tau}{\tau_*})\Big(1 + \frac{\tau_*}{\tau}\Big) + I_{\rm min} \qquad (1)$$

where the constants $(A, I_{\rm min}, \tau_{\rm temp})$ are $(0.2, 0.23, 62)$ for the yellow (dashed) curve and $(A, I_{\rm min}, \tau_{\rm perm})$ are $(0.33, 0.23, 100)$ for the pink (dotted) curve. As stated before, the bare (unfiltered, maximum) intensity $I_0 = 980$ mW/cm^2 at 535 nm. As expected we note that $\tau_{\rm temp} < \tau_{\rm perm}$. The variation in A reflects the fact that our experiments do not probe the $\tau \to 0$.

The recovery of organism motility when sustained exposure is not maintained has significant implications at the collective level. When light fields are spatially localized or patterned, fast moving cells have a higher chance of escaping exposure prior to complete paralysis. While swarming bacteria can reorient by run and tumble movements, motility driven by close bacteria-bacteria interactions dominate in a swarm. Thus slower cells are expected to be impacted more; first, because of longer exposure to the light and second, because they are more easily caged in and trapped by already paralyzed cells. In periodic fields, these persistence bacteria may also completely recover by the time they encounter the next exposed region. Exposure to insufficiently intense light or low exposure times may thus allow the faster cells that survive to eventually proliferate and dominate the population.

C. Phenomenology: Form and growth of the quenched region

To determine the extent of the quenched passivated domain, we use two threshold-based methods: the first utilizes image intensity fluctuations [40, 41] and the second utilizes PIV derived velocity fields. Our experiments were for the most part (unless stated otherwise) conducted at a filtered intensity of 3100 mW/cm^2 (measured at 535 nm[36]); exposure times were varied from 10-300 seconds.

The first method to extract the boundary of the quenched region uses point-wise fluctuations of the spatially varying intensity (I^*, distinct from the filtered maximum intensity)

$$|\Delta I^*(\mathbf{r}, t, \Delta t)| = |I^*(\mathbf{r}, t + \Delta t) - I^*(\mathbf{r}, t)|, \qquad (2)$$

where $I^*(\mathbf{r}, t)$ is the two-dimensional image intensity at pixel position $\mathbf{r}$ and Δt is the time step. We found that using $\Delta t = 0.1$ sec, which corresponds to the time in which a swarming *Serratia* cell swimming at 50 μm/s moves roughly a body distance (5 μm) provided good results; variations in Δt around this value (0.05 s $< \Delta t <$ 0.3 s) resulted in only small variations in results. To reduce noise in the system (due to pixel resolution, short-range fluctuations, and background light fluctuations), we filter pixel-wise $|\Delta I^*(\mathbf{r}, t, \Delta t)|$ by smoothing over 3x3 μm^2 areas. As shown in Fig. 3, the intensity fluctuations allow us to clearly identify and distinguish two domains, the immobile domain where values of $|\Delta I^*|$ are relatively small and the motile domain where $|\Delta I^*|$ are relatively large. Thresholding $|\Delta I^*|$ then yields the locus of points that defines the boundary of the active and passive phases. In the second method, the boundary position was obtained from coarse-grained spatially-averaged bacterial velocity fields from PIV (Fig. 3(b)); again, the exact boundary was defined using a threshold criterion [39]. The locations of the active and passive domains, as well as their relative sizes such as area, match between the two methods, although the intensity fluctuations identifies smaller features of the boundary compared to that from PIV. These metrics capture complimentary aspects of the swarm's motility: the intensity fluctuations are a scalar measure of density fluctuations and PIV yields vectorial velocity fields that quantify instantaneous polarity fields. In summary, simple thresholding using the inten-

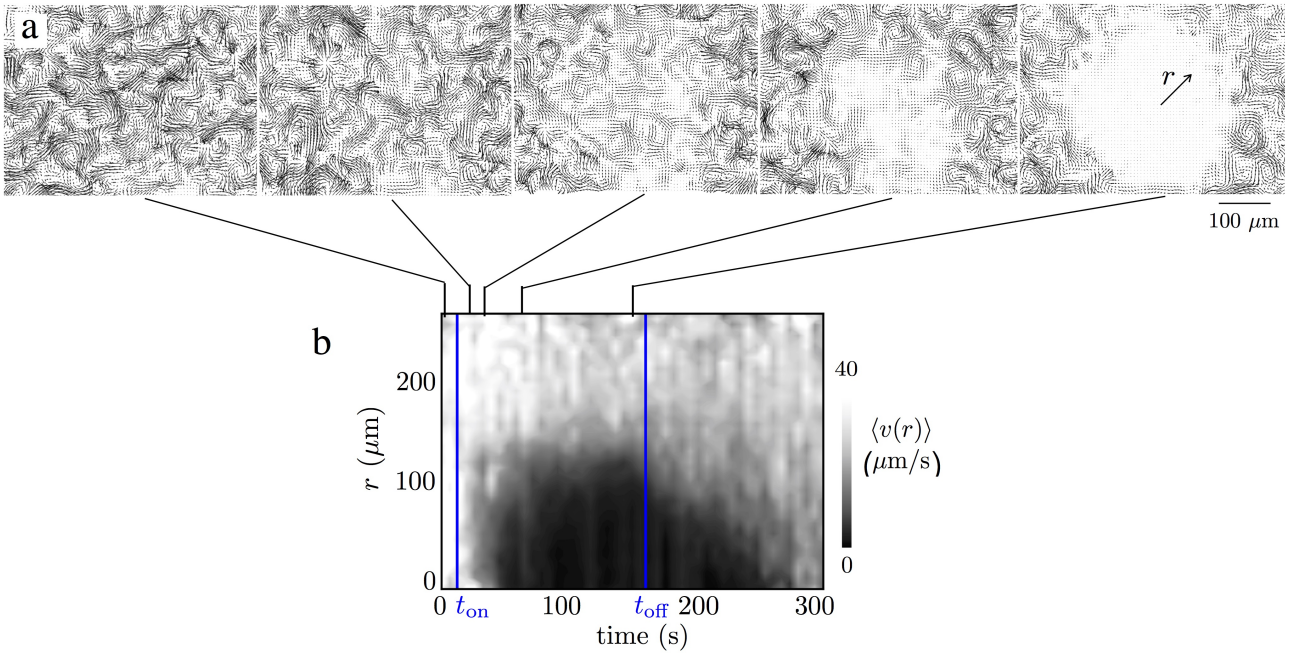

FIG. 4. **Thresholding using PIV derived fields:** (a) (Top) PIV derived bacterial velocity fields before and during light exposure. (Bottom) The azimuthally averaged velocity $\langle v \rangle$ highlights the creation of an immobile quenched domain within the exposed region. When the light is switched off, the active bacteria from the unexposed regions penetrate into the quenched domain, eroding it away. The filtered maximum intensity = 500 mW/cm^2. We note the brief lag after the light is switched on ($t_{\rm on}$), the gradual increase to a finite size as $t \to t_{\rm off}$ and the rapid erosion and mixing with the grey interphase region $t > t_{\rm off}$. The radial extent obtained by thresholding the intensity fluctuations also follows the square root dependence.

sity fluctuations and/or PIV derived velocity fields, yields physically meaningful boundary positions that separates the quenched region from the swarm. This approach can be formalized using phase-field approaches in order to extract the location and width of the interface[38, 39].

We next analyze the role of the exposure time τ that together with I determines the total light dosage, on the shape, size, and dissolution rate of the passive domain that is surrounded by the active swarm. Phenomenologically, exposure to light here is akin to quenching with activity *modified and in a sense removed* from our system. That is, exposure reduces the activity or energy in the system by removing the ability of bacteria to self-propel and inhibiting and eventually preventing large scale collective motions. Furthermore, as the bacteria slow down cell-cell steric interactions result in tightly jammed clusters with distinct aligned domains (Figure 3(a)). It is therefore of interest to examine the time-dependent velocity fields and the time-dependent growth of the passivated region.

In order to do this, we exploit the symmetry of the system and calculate a coarse-grained one-dimensional profile of the bacterial speed $\langle v \rangle$ by averaging over the azimuthal angle. This yields a velocity field that is a solely a function of the radial distance r from the center of the exposed region. Figure 4 shows a contour plot of the one-dimensional field $\langle v \rangle$ over time t and corresponding snapshots of the two-dimensional velocity field. The passive domain appears in the contour plot (Fig. 4b) as the dark region where the bacterial speed is zero.

When the light source is turned on, the bacterial speed in the exposed region decreases in a non-uniform manner, diminishing the most in the center of the exposed region (Fig. 4a). The two dimensional velocity fields suggest that bacteria stop moving in multiple sub-domains, each of which continuously interact with active bacteria that are still moving. It takes approximately 50 seconds of exposure for a spatially-uniform passive domain to develop. In the swarming state, the motion of individual *Serratia marcescens* may be decoupled into a mean velocity (with long range correlations arising from collective motions) and a diffusion-like term dependent on bacterial diffusivity and on steric cell-cell interactions. We hypothesize that the delay we observe time in going from the temporarily passive to fully immobile phase is a consequence of slow and differing time scales over which collective speeds and diffusivities decrease. Both these trends result in the slowly deactivating bacteria experiencing increasing jammed situations with local flocks aligning. Once this initial quenched domain forms (after the initial lag time $t_{\rm lag}$), the size of the passive domain increases monotonically with time t. Fluctuations in the calculated extent of the quenched domain may arise physically due to variations in the (averaged) heterogeneous, fluctuating velocity fields during exposure (Fig. 4a) that result in momentum boundary layers at the edge; a small

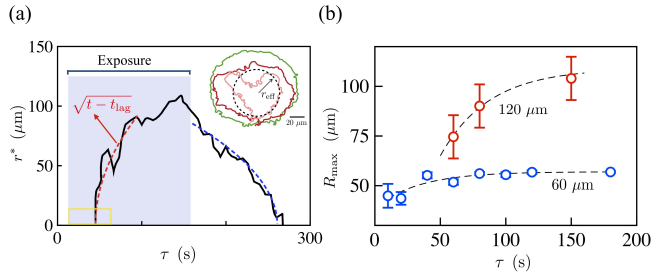

FIG. 5. **Growth, shape and dissolution of the quenched domain:** (a) The effective size of the quenched region grows during exposure, stabilizes while illuminated asymptotes to a constant and then decreases to zero once the light is switched off. We calculate the effective radius of the quenched region r^* defined by the locus of points satisfying $\langle v\rangle(r^*) = 10$ μm/s and examine its dependence as a function of time. When the light source is turned on at $t_{\rm on}$, this radius increases from zero only after an apparent lag time $t_{\rm lag} \approx 50$s. Lowering the threshold velocity yields a noisier initial growth region with shorter lag. The initial growth has a square root dependence with time (red dashed curve). We observe deviations of around $5-10$ μm in these curves due to variations in the velocity field. The aperture size used here is 120 μm. (Inset) Interface shapes of the quenched (passive) region obtained from thresholding intensity fluctuation fields; we define $r_{\rm eff}$. Pink, red and green curves correspond to exposure times of 10, 20 and 100 seconds (aperture size 60 μm, 20x objective). (b) The maximum effective size of the passive phase $R_{\rm max}$ increases with exposure duration τ and asymptotes to a constant that is less than the aperture size.

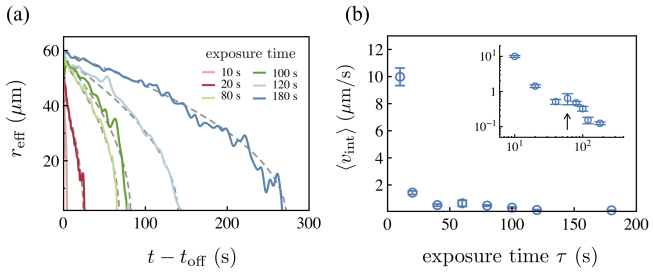

FIG. 6. (a) The effective extent of the quenched, passive domain decreases over time t at rates that depend on the exposure duration τ reflecting the influence of the alignment effects due to jamming as the bacteria are exposed to light. Longer exposure times prolong erosion by the active swarming bacteria, increasing the time it takes for the passive phase to disappear (at time t_0). For each τ, the effective size $r_{\rm eff}$ follows $r_{\rm eff} \approx \sqrt{t_0 - t}$ (grey dashed curves) with $t_0(\tau)$ being the time for complete dissolution. (b) The average initial dissolution velocity $\langle v_{\rm int}\rangle$ decreases significantly with τ. Data is the average calculated from four experiments with standard deviation as error bars (Intensity ≈ 3 W/cm^2).

part of these variations may also arise from the threshold criterion selected.

When the light is turned off, active bacteria penetrate the passive phase and convect passive bacteria away. The advancing swarm intermingles with the passivated bacteria as it propagates inward - this increases the average bacterial speed indicated in the PIV as seen in Fig. 4b. In approximately 100 seconds post exposure, the active swarm recaptures the exposed domain. We note that the boundary layer at the edge of the rapidly eroding quenched domain is larger than when the domain is being formed.

The effective size of the quenched domain in Fig. 4b can be estimated by thresholding the values of $\langle v\rangle$. We use a threshold of 10 μm/s - this value is much less than the average speed of the active region (40 μm/s) while large enough to average over small fluctuations. Adjusting for the lag time, we find that the radius of the quenched region $r^* \approx \sqrt{T}$ (Figure 5) where $T = t - (t_{\rm lag} + t_{\rm on})$ with $t_{\rm on}$ being the time when the light source is turned on. Large variations in r^* are a consequence of asymmetric formation of the passive domain. The square-root dependence is a better fit to data when the passive domain starts to form but is not as good a fit as the passive domain saturates to a radial extent slightly less than the size of the exposed region (120 μm). We note that this estimate of the quenched region obtained from using the velocity field is ≈ 5 μm less than that obtained from using the intensity fluctuation fields. Nevertheless, the square root dependence on time approximately holds for both estimates.

In plotting the data for the growing domain in Figure 5, we ignored variations in motility inside the domain being exposed. Consequently, it is difficult to directly assign a physical mechanism behind the square root growth of the exposed domain. In our experiments on the swarm, quenching due interaction between the bacteria and the light field effectively extracting the actively generated energy of the swarm by degrading the ability of the bacteria to move and self-propel. If the mean velocity of the swarm arising due to the propagation of the swarm front is ignored, then one can treat the fluctuating swarm velocities, $\mathbf{v}$, as time-varying fields with a zero mean when suitably averaged. The dyadic tensor $\mathbf{vv}$ then encodes information about the *energy content of the swarm*. Averaging over times scales long enough to encompass multiple vortex and streamer lifetimes, and then averaging azimuthally about the polar angle in the swarming plane, we can obtain a radially dependent scalar field $\Psi(r,t) \equiv \sqrt{\langle\langle|\mathbf{v}|^2\rangle\rangle}$. In principle, the evolution of this quantity is coupled to the position dependent light field. While more experiments are require to formulate equations governing $\Psi(r,t)$, it is interesting to compare the dynamics we observe with that in a much simpler, albeit similar physical problem - the one-dimensional freezing of a domain due to a heat sink at the origin that also yields a square root dependence in time for the boundary of the frozen domain (Appendix A).

D. Exposure time determines maximum size of quenched domain

Next, we examine the differences in the shape and maximum size of the quenched domains that form as a function of the exposure times τ (Figures 6a and 6b). To adjust the viewing window, the 60 μm aperture experiments are done with a 20x objective and the 120 μm aperture with a 10x objective (we take into account the higher value for the intensity for the 60 μm aperture case at 20x). To quantify the mean and variance of the data, we plot the average from four experiments with corresponding to the standard deviation shown as error bars. Aiming to obtain a upper bound on the extent of the swarming domain that is impacted, we choose to use intensity fluctuation fields rather than the PIV derived velocity fields. Thus we track the un-averaged boundary positions $\mathbf{r}_{\rm I}(t)$ from the image intensity fluctuations $|\Delta I^*|$ using Equation 2. We then estimate the effective size of the passive phase $r_{\rm eff}$ by calculating the radius of gyration of the boundary positions following

$$r_{\rm eff}(t) = \sqrt{\int_{\rm Passive} |\mathbf{r}_{\rm I} - \overline{\mathbf{r}}|^2 \, d\mathbf{r}} \qquad (3)$$

where $\overline{\mathbf{r}}$ is the center of mass at time t. The maximum extent of the passive phase $R_{\rm max}$ is equal to $r_{\rm eff}(t = t_{\rm off})$; here the time at which exposure is terminated is $t_{\rm off}$.

From Figure 6a (aperture size 60 μm), it is clear that exposure times result in incompletely quenched and irregular, asymmetric domains. As the exposure time is increased, the domains become larger (eventually comparable to the aperture size) and more regular. The maximum intensity of light is at the center of the aperture and so the quenching starts there with the boundary propagating outward. The domain size $r_{\rm max}$ increases with τ and asymptotes to a constant that is slightly less than the aperture size (Fig. 6b); the asymptote is approximately 58 μm for the 60 μm aperture. For aperture size 120 μm, we find the limiting asymptote to be ≈ 109 μm. The data in Fig. 6b fits the functional form

$$r_{\rm max} = r_{\rm F}\left[1 - \frac{b}{r_{\rm F}} \exp\left(-\frac{\tau}{\tau_c}\right)\right], \qquad (4)$$

with $r_{\rm F} = 58$ μm, $b = 18$ μm, and $\tau_c = 33.5$ s for the 60 μm aperture and $r_{\rm F} = 109$ μm, $b = 169$ μm, and $\tau_c = 37.3$ s for the 120 μm aperture. As mentioned earlier, the erosion of the quenched domain once exposure is stopped seems to follow a square root dependence until the domain disperses completely at time t_0; this feature is next examined for various exposure times, τ (Figure 7a). Surprisingly, we find that the square-root scaling hold for both small as well as long exposure times. The time scale t_0 increases with exposure time. In our active, far-from equilibrium system, the passive domain is eroded by single bacteria-bacteria interactions (displacements originating from steric and self-propulsive mechanisms) as well as by collective highly non-equilibrium flow structures that form near the surface. Elucidating the origin of this scaling requires a consideration of the coupling between interface shape, interface speed and interface flow fields [39].

Finally, we also measure the initial boundary dissolution speed by calculating $\langle v_{\rm int}\rangle = \big(r_{\rm eff}(t_{\rm off}) - r_{\rm eff}(t_{\rm off} + \Delta t)\big)/\Delta t$, where $\Delta t = 10$ seconds. We find that $\langle v_{\rm int}\rangle$ varies significantly with exposure time (Figure 7b), decreasing from 10 μm/s to 0.1 μm/s as τ increases from 10 to 300 seconds. The decrease in speed is not monotonic, rather we observe a peak (inset) that is not ascribable to experimental variations. For long exposure times or high intensities, as the exposed bacteria are slowly paralyzed and slow down, they form jammed, highly aligned domains. Thus the time for complete erosion will be larger due to both the larger extent to be eroded as well as the aligned caged configurations of paralyzed bacteria.

IV. DISCUSSION AND PERSPECTIVES

The motion of dense bacterial suspensions or swarming bacterial can be impacted by light in two ways - 1) at the level of single organisms where light can direct impact the bio-molecular and biochemical mechanisms underlying flagellar propulsion and tumbling and therefore both speed and effective diffusivity, and 2) at the collective level, where small regions of immobile bacteria can can both effectively blocking parts of space accessible to swarms as well as trap motile bacteria, thereby prevent them from escaping the light and eventually forming large quenched jammed domains.

We find that the *collective motility* of swarming *S*erratia marcescens displays a range of behaviors in response to wide-spectrum light rich in UV wavelengths. At minimum exposure levels, swarms withstand the effects of light on their ability to move and maintain long-range collective motions. For sufficiently intense exposures, bacteria are rendered immobile and paralyzed, an effect that is either reversible or irreversible, depending on the exposure level. The passive domain occurs for critical values of illumination power, requiring a minimum exposure time to appear. Longer exposure times prolongs the dissolution of the passive phase by the active swarming bacteria. Note that local weakly interacting, high aspect ratio passive polar rods in the dense passive phase can organize into stable as well as metastable highly ordered states through thermal motions augmented by steric interactions [42] or other weakly aligning interactions [43]. The slowing of individual bacteria, disruption of their self-propulsion and the further orienting affects of local shearing motions by neighboring bacteria may allow the same mechanisms to operate here and result in the formation of strongly aligned and jammed phases.

In the absence of UV exposure, the swarming bacteria exhibit collective flows with significant vorticity interspersed with streaming motions. At a minimal level, let

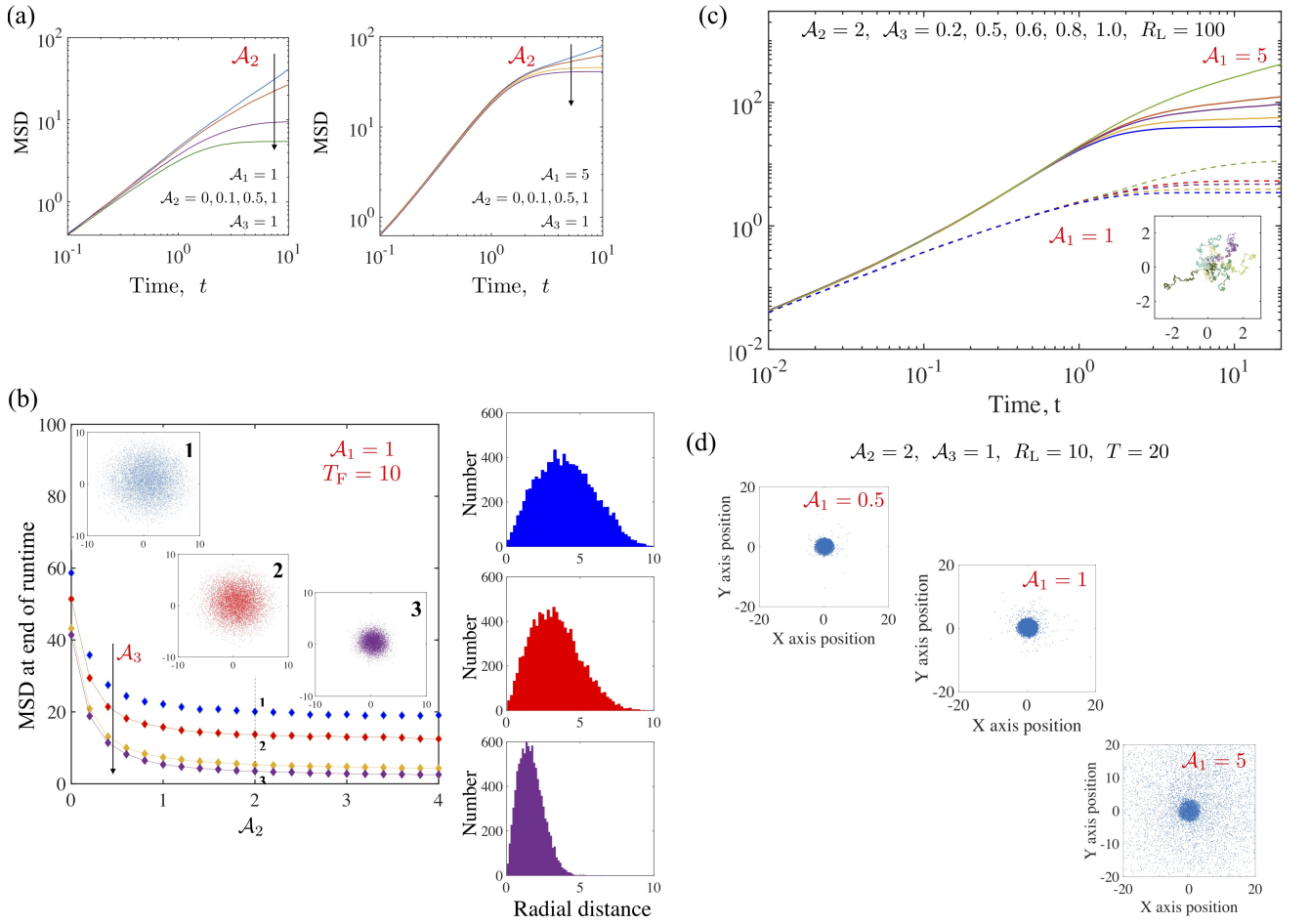

FIG. 7. (Left - a,b) Dynamics of diffusing particles ($N = 10^4$) interacting with a constant, unbounded light field ($\Phi(\mathbf{r}) = 1$, $R_L = \infty$) that deactivates them. Trajectories are integrated till dimensionless time T_F using $\Delta t \in (4 \times 10^{-4}, 10^3)$. (a) Dimensionless ensemble averaged MSD(t) shows trajectories becoming denser and compact. Changes in both diffusivities are required for this to happen, provided $\mathcal{A}_3 > 0$. The larger the value of the Peclet number $\mathcal{A}_1$, the longer the particles travel before effects become pronounced. (b) MSD($t = T_F$) as a function of $\mathcal{A}_2$ for various values of $\mathcal{A}_3$ (from top to bottom: 0.1, 0.5, 1 and 2) with $\mathcal{A}_1 = 1$. We observe that for $\mathcal{A}_2 > 3$, the MSD saturates. Higher values of $\mathcal{A}_3$ implies (exponentially) higher rates of reorientation and a decrease in the MSD. (Inset) Shown are the (x, y) locations of the particles for parameters corresponding to points 1, 2 and 3 marked on the plot. Examination of the corresponding number distribution plots shows a peak that shifts to lower values of radial distance $r(t = T_F)$, and significant changes to the tail end of the distribution function. Since the light field is unbounded, all particles are eventually affected. Thus for particles with low Peclet number (low activity), the exposure time determines how far they can travel before becoming deactivated. (Right - c,d) Here we explore the effects of an imposed length scale R_L using a position dependent light field $\Phi(\mathbf{r}) = 1\ \forall r \in (0, R_L)$ and zero elsewhere. We integrate trajectories of 10^4 particles using $\Delta t = 4 \times 10^{-4}$ up to final times T_F. (c) First effects of finite light extent. The dimensionless MSD is shown as a function of time for $R_L = 100$. Solid curves are results for $\mathcal{A}_1 = 5$ while dashed curves are for $\mathcal{A}_1 = 1$. We see that as $\mathcal{A}_3$ increases from 0.2 to 1.0, MSD saturates rapidly. (Inset) Sample trajectories for $\mathcal{A}_1 = 1$ for $0 \leq t \leq 20$ indicating that the particles are rapidly localized for $t > 6$. (d) Snapshots of the positions of the cells at $t = 20$. For fixed R_L - here, set at 10 - faster particles (increasing $\mathcal{A}_1$) are able to escape the light field. Thus the fraction of the total cell population that can escape to beyond R_L increases with increasing $\mathcal{A}_1$. Note that here we have assumed that the light interacts by increasing tumbling rates and therefore increased orientational diffusion. Alignment effects could alternately impact both translational and rotational diffusion negatively and reduce them to negligible values; in this case cells can cease to move by jamming as happens when encountering domains with a different orientation.

us consider vortical motions as corresponding to reorientations and streaming motions as corresponding to effective self-propulsion. At large time scales then, we may idealize motions as corresponding to *test particles* continuously diffusing in time and space. This is of course a highly reduced picture - in reality, swarming bacteria have complex motions and two adjacent bacteria may be separated by a very large distance spanning multiple vortices later in time. In the exposed region however, these diverging trajectories are continually minimized due to

the slow paralysis induced by light exposure and deactivation. To incorporate the effects of light, we appeal to our experimental observations and those of Lu *et. al.*[30]. We assume that light exposure increases the effective rotational diffusivity of the idealized test cells - this may arise for instance from increased tumbling. At the same time, as the test cell moves in a mean field of its co-deactivating neighbors, its translational diffusion is expected to slow down due to crowding and alignment induced hindering. The cell of course experiences different environments perpendicular and normal to its polar orientation, but we will assume that anisotropy in anisotropic diffusion coefficients is not as important as the fact that the diffusion slows down. Here motivated by these observations, we study a very simple, minimal model (details in Appendix B) that focusses on features of the deactivation process that is not accessible from our experiments; namely, the factors that influence the escape of trapped bacteria from the light field. The generalized Langevin equations for the dynamics of an idealized cell can be scaled to obtain three dimensionless parameters. These are the Peclet number $\mathcal{A}_1$ charactering the self propulsion at the single cell level and two deactivation parameters - $\mathcal{A}_2$ and $\mathcal{A}_3$ - that quantify how the light affects translational and rotational diffusion. Salient results summarized in Figure 7 show that, for this minimal model, the Peclet number controls how far particles travel before losing mobility in an unbounded light field. In a bounded light field of extent $R_{\rm L}$, the Peclet number also determines the fraction of cells that can escape the light field. For bacteria with fixed propulsion and response at the organismal level, this implies that the time of exposure controls the fraction of cells immobilized. We are currently studying the quenching process using detailed agent based simulations that account for the rod geometry of the bacteria, hydrodynamic interactions (by modeling the bacteria as force dipoles) and excluded volume interactions via the Maier-Saupe potential that builds on this minimal model.

A natural extension of our experiments would be to systematically isolate the effects of light on different aspects that determine swarm survival and virulence including individual cell motility, collective motion and active/passive particle interactions [44]. When exposed bacteria are rendered permanently immobile, jammed passive bacteria may act as a physical barrier and hinder the flux of unexposed bacteria; thus only a small fraction of the bacteria that are directly exposed are disinfected. Furthermore, evolution through mutation and selection in natural bacterial populations allow bacterial populations to differentiate genetically and phenotypically and better adapt to the damaging effects of light. Bacteria that are able to recover may be genetic variants predisposed to UV resistance. Reestablishing collective motility, and upon subsequent cell divisions, these cells may eventually result in emergence of resistant strains. Experiments using filters that allow for wavelength dependent immobilization at the single cell level will allow us to further understand how to collective motility and light exposure are related. Our results thus complement previous studies on the effects of light on planktonic bacteria and inform models of light-driven patterning in clusters of deactivating bacteria.

ACKNOWLEDGEMENTS

We thank Ed Steager and Elizabeth Hunter for providing the cells and for experimental assistance. PEA acknowledges funds from NSF-DMR-1104705 and NSF-CBET-1437482. AEP was supported by an NSF Graduate Research Fellowship. AG acknowledges startup funds from the University of California, Merced.

APPENDIX A: FREEZING IN ONE DIMENSION

Within the framework of sharp interface formulations, the governing equations for the one dimensional freezing problem we consider can be written in a form that involves a continuous scalar field (here, the temperature) and its derivatives. At the moving boundary between the frozen (solid) and mobile (liquid) phases, we impose a Stefan boundary condition that relates the motion of the boundary to the derivative of the scalar field.

Let us define a continuous field $\Psi(X,t)$, with $0 \leq X < \infty$ here being a suitable one dimensional coordinate and t the time. At the origin $X = 0$, we impose $\Psi = \Psi_0 < \Psi_{\rm m}$ for all $T \equiv t - t_{\rm ini} > 0$, where $\Psi_{\rm m}$ is the equilibrium value at which freezing/melting occurs and $t_{\rm ini}$ is the time at which solidification starts at $x = 0$. For simplicity, the liquid phase is assumed to be all at $\Psi = \Psi_{\rm m}$. This approximation is the limiting case of thermal diffusivities in the liquid being much larger than in the solid. For small solidification rates and zero surface tension, the interface $X^*(t)$ separating the solid and liquid phases satisfies $\Psi(X = X^*, t) = \Psi_{\rm m}$.

The coupled equations that govern the freezing dynamics of the field Ψ may be written in the form (5)-(9) below and solved using similarity variables with closed-form solutions [45, 46] (8)-(9) involving the error function (erf),

$$\frac{\partial \Psi}{\partial T} = \alpha \frac{\partial^2 \Psi}{\partial X^2}, \quad X \leq X^*, \tag{5}$$

$$\Psi(0, T > 0) = \Psi_0 < \Psi_{\rm m}, \quad \Psi(X, 0) = \Psi_{\rm m}, \tag{6}$$

$$\Psi(X > X^*, T > 0) = \Psi_{\rm m}, \quad \frac{dX^*}{dT} = \beta \frac{\partial \Psi}{\partial X}(X^*, T), \tag{7}$$

$$\Psi(X, T) - \Psi_0 = (\Psi_{\rm m} - \Psi_0) \frac{\mathrm{erf}\left(X/2\sqrt{T\alpha}\right)}{\mathrm{erf}(\gamma)} \tag{8}$$

$$X^*(T) = 2\gamma\sqrt{\alpha T}, \tag{9}$$

with $\gamma \ \exp(\gamma^2)\,\mathrm{erf}(\gamma) = \alpha(\Psi_m - \Psi_0)/\beta\sqrt{\pi}$.

APPENDIX B: DYNAMICS OF A SELF-PROPELLING PARTICLE DEACTIVATED BY LIGHT

We simulate $N = 10^4$ trajectories of self-propelling independent polar particles moving in an incident light field $I_{\rm in}(\mathbf{r}) = I_0\Phi(\mathbf{r})$ on a plane. The particles start from the origin in all realizations; we then track their trajectories as they self-propel and move while interacting with the light at all times. We assume over-damped dynamics; the ambient fluid exerts purely viscous forces and torques on the cell proportional to instantaneous velocities. The center of mass of a test particle is located at $\mathbf{r}_p$ and the unit vector corresponding to the orientation of its head and the direction of self-propulsion is $\mathbf{u}$; the particle moves along the preferred direction $\mathbf{u}$ with constant speed v_c. The two-dimensional trajectory governing the evolution of the test particle moving on the $x-y$ plane follows from Langevin equations for the translation and rotary motion

$$\partial_t \mathbf{r}_p = v_c\mathbf{u} + \boldsymbol{\eta}^T(t) \tag{10}$$

$$\partial_t \mathbf{u} = \boldsymbol{\eta}^T(t). \tag{11}$$

that incorporate noise and diffusivity via terms $\boldsymbol{\eta}^T(t)$ and $\boldsymbol{\eta}^R(t)$. In the limit of an equilibrium diffusing particle that is not affected by the light source, these terms would be directly related to the friction constants and diffusion constants following the equipartition and fluctuation-dissipation theorems.

Here to make progress and keep the model simple, we will build on this picture and assume that the diffusivities are modified from the bare equilibrium values by a term that depends on time. Thus we write $\left\langle \boldsymbol{\eta}^T(t)\,\boldsymbol{\eta}^T(t')\right\rangle = D_{\rm T}^o F(t)\ \mathrm{I}\ \delta(t-t')$ and $\left\langle \boldsymbol{\eta}^R(t)\,\boldsymbol{\eta}^R(t')\right\rangle = D_{\rm R}^o G(t)\,\mathrm{I}\,\delta(t-t')$ with the time dependent factors $F(t)$ and $G(t)$ incorporating the slow deactivation of the self-propelling, diffusing particle in time due to light exposure as well as possible effects of trapping as the test cell is hindered (in a mean field sense) by its neighbors (all of whom are also slowly deactivating in time). Here, δ is the Kronecker delta function while $\mathbf{I}$ is the identity tensor in two dimensions.

For the test particles, the rotational diffusivities are related to the time for which its direction is correlated - so that $D_{\rm R}^o \sim \tau_c^{-1}$. The ensemble averaged mean square displacement at time t, MSD(t) corresponding to trajectories satisfying (10) and (11) can be obtained in closed form (consistent with previous results [47]):

$$\mathrm{MSD}(t) = \left(\frac{v_c}{D_{\rm R}^o}\right)^2\left[\left(\frac{2\sqrt{D_{\rm T}^o D_{\rm R}^o}}{v_c}\right)^2 t + D_{\rm R}^o t + \frac{1}{2}\left(\mathrm{e}^{-2tD_{\rm R}^o}-1\right)\right]. \tag{12}$$

In the most general case to simulate the deactivation by light exposure, we first scale the dimensional equations. Here we choose to separate the role of self-propulsion (activity) from the physical hindering effects as the cell is deactivated; therefore, we choose the time scale $\tau_c \equiv 1/D_{\rm R}^o$ and the length scale $\ell_c \equiv \sqrt{D_{\rm T}^o\tau_c}$ to render the governing equations (10) and (11) dimensionless. The equation for the polarity can be written in terms of an angular variable - the polar angle θ, chosen to be the angle made by $\mathbf{u}$ with the unit vector along the x axis $\mathbf{e}_x$ where $\mathbf{t}$ is the tangent vector orthogonal to $\mathbf{u}$. Thus $\mathbf{u}\cdot\mathbf{e}_x = \cos\theta$. We next decompose (12) into its cartesian components, write (10) and (11) in terms of the angle θ and define the dimensionless Peclet number, $\mathcal{A}_1 \equiv (v_o\tau_c/\ell_c)$. The discrete version of the Langevin equations (10) and (11) in the Euler-Maruyama implementation then has the form (in simulation units) (here $n+1$ is the time index with associated time stamp $t_{n+1} = t_n + \Delta t$)

$$x_{n+1} = x_n + \Delta t\,\mathcal{A}_1\cos\theta_n + \sqrt{2F_1(t_n)\Delta t}\mathcal{N}_1 \tag{13}$$

$$y_{n+1} = y_n + \Delta t\,\mathcal{A}_1\sin\theta_n + \sqrt{2F_2(t_n)\Delta t}\mathcal{N}_2 \tag{14}$$

$$\theta_{n+1} = \theta_n + \sqrt{2F_3(t_n)\Delta t}\mathcal{N}_3. \tag{15}$$

Here $\mathcal{N}_1$, $\mathcal{N}_2$ and $\mathcal{N}_3$ are normally distributed random variables with mean 0 and standard deviation 1. Equations (13)-(14) constitute a first-order integration method and necessitate a small time step Δt.

To incorporate the effects of light, we appeal to experimental observations. The effect of light on *Bacillus subtilis* [30] in the presence of photosensitizer reveals that as the bacterial cells become sluggish, the tendency to form flocks and large packs reduces and instead smaller clusters are observed. The overall reduction in cluster size and a less ordered motion within individual clusters gives rise to decreased correlation lengths with swarming eventually reverting to random motion in the presence of photodynamic effects. Consistent with these observations and our experimental results, we assume that light exposure increases the effective rotational diffusivity $D_R^o F_3$ of our test cell (that may arise for instance from increased tumbling in bacteria). At the same time, as the test cell moves in a mean field of its co-deactivating neighbors, its translational diffusion is expected to slow down due to crowding and alignment induced hindering. The cell of course experiences different environments perpendicular and normal to its polar orientation, but we will assume that anisotropy in anisotropic diffusion coefficients is not as important as the fact that the diffusion slows down. Keeping these features in mind, we write

$$F_1(t) = F_2(t) = \exp\left(-\mathcal{A}_2\int_0^t \Phi(\mathbf{r}^\alpha(t'),t')\ dt'\right) \tag{16}$$

$$F_3(t) = \exp\left(\mathcal{A}_3\int_0^t \Phi(\mathbf{r}^\alpha(t'),t')\ dt'\right) \tag{17}$$

where the dimensionless parameters $\mathcal{A}_2$ and $\mathcal{A}_3$ characterize the deactivation process. Note that as $t\to\infty$, F_1 and F_2 both tend to zero. We study predictions of equations (13)-(17) for two cases. The first case is for uniform unbounded light field so that $\Phi(\mathbf{r}) = 1$ so that $F_1(t) = F_2(t) = \exp(-\mathcal{A}_2 t)$ and $F_3(t) = \exp(\mathcal{A}_3 t)$ so

that $F_{1,n} = F_{2,n} = \exp(-\mathcal{A}_2 t_n)$ and $F_{3,n} = \exp(\mathcal{A}_3 t_n)$. The second case we consider is a localized light field of the form $\Phi(\mathbf{r}) = 1\ \forall r \in (0, R_{\mathrm{L}})$ and zero elsewhere. We integrate equations (13)-(17) for a dimensionless time of between 10^{-1} to 20 with Δt varying from 10^{-3} to 10^{-4} to check for consistency and convergence.

[1] L. Alberti and R. M. Harshey, *Journal of bacteriology*, 1990, **172**, 4322.
[2] R. M. Harshey, *Annual Reviews in Microbiology*, 2003, **57**, 249.
[3] N. Verstraeten, *Trends in microbiology*, 2008, **16**, 496.
[4] M. F. Copeland and D. B. Weibel, *Soft matter*, 2009, **5**, 1174.
[5] N. C. Darnton *et al. Biophysical journal*, 2010, **98**, 2082.
[6] L. Turner, R. Zhang, N. C. Darnton and H. C.. Berg, *Journal of bacteriology*, 2010, **192**, 3259.
[7] D. B. Kearns, *Nat. Rev. Microbiol.*, 2010, **8**, 634.
[8] R. M. Harshey and J. D. Patridge, *Journal of molecular biology*, 2015, **427**, 3683.
[9] E. B. Steager, C. B. Kim and M. G. Kim, *Physics of Fluids*, 2008, **20**, 073601.
[10] M. T. Butler, Q. Wang and R. M. Harshey, *Proceedings of the National Academy of Sciences.*, 2010, **8**, 3776.
[11] D. Roth *et al*, *Environmental microbiology*, 2013, **15**, 2532.
[12] S. Lai, J. Trembley and E. Deziel, *Environmental microbiology*, 2009, **11**, 126.
[13] C. Chen, S. Liu, X. Shi, H. Chate and Y. Wu, *Nature*, 2017, **542**, 210.
[14] H. C. Berg and D. A. Brown, *Nature*, 1972, **239**, 500.
[15] H. C. Berg, *E. coli in Motion*. 2008, Springer.
[16] G. H. Wadhams and J. P. Armitage, *Nat. Rev. Mol. Cell Biol.*, 2004, **5**, 1024.
[17] H. C. Berg and R. A. Anderson, *Nature*, 1973, **245**, 380.
[18] A. E. Patteson, A. Gopinath, M. Goulian and P. E. Arratia, *S*cientific Reports, 2015, **5**, 15761.
[19] B. L. Taylor and D. E. Koshland Jr., *Journal of bacteriology*, 1975, **123**, 557.
[20] S. Wright *et. al.*, *Journal of bacteriology*, 2006, **188**, 3961.
[21] E. Steager *et. al.*, *Applied Physics Letters*, 2007, **90**, 26.
[22] M. P. Conley and H. C. Berg, *Journal of bacteriology*, 1984, **158**, 832.
[23] V. Kodoth and M. Jones, http://medicalmate.gr/img/cms/UVC, 2015, 1.
[24] L. Alonso-Saez, J. M. Gasol, T. Lefort, J. Hofer and R. Sommaruga, *Appl Environ Microbiol.*, 2006, **72**(9), 5806.
[25] D. G. Sharp, *J. Bacteriol.*, 1940, **39**(5), 535.
[26] M. B. Said, S. Khefacha, L. Maalej, I. Daly and A. Hassen, *African J. of Microbiol. Res.*, 2011, **5**(25), 4353.
[27] B. Li and B. E. Logan, *Colloids Surf B Biointerfaces*, 2005, **41**(2-3), 153.
[28] C. M. Abana *et. al.*, *Microbiologyopen.*, 2017, **6**(4), e00466.
[29] T. Dai, M. S. Vrahas, C. K. Murray and M. R. Hamblin, *Expert review of anti-infective therapy*, 2012, **10**, 185.
[30] S. Lu, W. Bi, X. Wu, B. Xing and E. K. L. Yeow, *Phys. Rev. Lett.*, 2013, **111**, 208101.
[31] T. Dai *et. al.*, *Antimicrobial agents and chemotherapy*, 2013, **57**, 1238.
[32] S. Pei, A. C. Inamadar, K. A. Adya and M. M. Tsoukas, *Indian Dermatol Online J.*, 2015, **6**, 145.
[33] S. Bensity E. Ben-Jacob, G. Ariel and A. Be'er, *Phy. Rev. Lett.*, 2015, **114**, 018105.
[34] A. E. Patteson, A. Gopinath and P. E. Arratia, *Current Opinion in Colloid & Interface Science*, 2016, **21**, 86.
[35] W. Thielicke and E. Stamhuis, *Journal of Open Research Software*, 2014, **2**, 1.
[36] http://zeiss-campus.magnet.fsu.edu/print/lightsources/mercuryarc-print.html
[37] Y. Wu and H. C. Berg, *Proc. Nat. Acad. Sci.*, 2011, **109**, 4128.
[38] A. Gopinath, R. C. Armstrong and R. A. Brown, *J. Cryst. Growth*, 2006, **291**(1), 272.
[39] A. E. Patteson, A. Gopinath and P. E. Arratia, bioRxiv 324251; doi: https://doi.org/10.1101/324251.
[40] R. Cerbino and V. Trappe, *Physical Review E*, 2008, **80**, 031403.
[41] L. G. Wilson *et. al.*, *Phys. Rev. Lett.*, 2011, **106**, 018101.
[42] A. Gopinath, R. C. Armstrong and R. A. Brown, *J. Chem. Phys.*, 2004, **18**, 028102.
[43] A. Gopinath, L. Mahadevan and R. C. Armstrong, *Phys. Fluids*, 2006, **121** (12), 6093.
[44] A. E. Patteson, A. Gopinath, P. K. Purohit and P. E. Arratia, *Soft Matter*, 2016, **12**(8), 2365.
[45] H. S. Carslaw and J. C. Jaeger, *Conduction of heat in solids*, 1959, Oxford Science, 2nd edition.
[46] G. Barenblatt, *Scaling, Self-similarity, and Intermediate Asymptotics: Dimensional Analysis and Intermediate Asymptotics*, 1996, Cambridge University Press.
[47] G. Volpe, S. Gigan and G. Volpe, *Am. J. Physics*, 2014, **82**, 659.